

Disruption of Aquaporin-11 Produces Polycystic Kidneys following Vacuolization of the Proximal Tubule

Yoshiyuki Morishita,¹ Toshiyuki Matsuzaki,² Mariko Hara-chikuma,³ Ayaka Andoo,⁴ Mariko Shimono,⁴ Asako Matsuki,⁵ Katsuki Kobayashi,⁷ Masahiro Ikeda,⁴ Tadashi Yamamoto,⁵ Alan Verkman,³ Eiji Kusano,¹ Shigeo Ookawara,¹ Kuniaki Takata,² Sei Sasaki,⁶ and Kenichi Ishibashi^{1,6,7*}

Department of Nephrology and Anatomy, Jichi Medical School, Tochigi 329-0498, Japan¹; Department of Anatomy and Cell Biology, Gunma University Graduate School of Medicine, Maebashi, Gunma 371-8511, Japan²; Cardiovascular Research Institute, UCSF, San Francisco, California 94143-0521³; Department of Veterinary Pharmacology, University of Miyazaki, Miyazaki 889-2192, Japan⁴; Institute of Nephrology, Niigata University Graduate School of Medical and Dental Science, Niigata 951-8510, Japan⁵; Department of Nephrology, Tokyo Medical and Dental University, Tokyo 113-8591, Japan⁶; and Clinical Research Center, Chiba-East National Hospital, Chiba 260-8712, Japan⁷

Received 18 March 2005/Returned for modification 6 May 2005/Accepted 9 June 2005

Aquaporin-11 (AQP11) has been identified with unusual pore-forming NPA (asparagine-proline-alanine) boxes, but its function is unknown. We investigated its potential contribution to the kidney. Immunohistochemistry revealed that AQP11 was localized intracellularly in the proximal tubule. When AQP11 was transfected in CHO-K1 cells, it was localized in intracellular organelles. AQP11-null mice were generated; these mice exhibited vacuolization and cyst formation of the proximal tubule. AQP11-null mice were born normally but died before weaning due to advanced renal failure with polycystic kidneys, in which cysts occupied the whole cortex. Remarkably, cyst epithelia contained vacuoles. These vacuoles were present in the proximal tubules of newborn mice. In 3-week-old mice, these tubules contained multiple cysts. Primary cultured cells of the proximal tubule revealed an endosomal acidification defect in AQP11-null mice. These data demonstrate that AQP11 is essential for the proximal tubular function. AQP11-null mice are a novel model for polycystic kidney diseases and will provide a new mechanism for cystogenesis.

Aquaporins (AQPs) are a family of membrane proteins that facilitate the transport of water and small solutes (8, 15, 21). They are distributed widely in nature from bacteria to animals. Eleven aquaporins (AQP0 to AQP10) have been identified and functionally characterized in humans. We reported the most recent AQP, AQP10 (11, 13). Their physiological importance is documented by the targeted disruption in mice (knock-out mice) and by the discovery of humans and mice with nonfunctioning mutations. Of nine AQPs disrupted in mice and humans (AQP0 to AQP7 and AQP10), only AQP2-null mice die due to massive polyuria from nephrogenic diabetes insipidus (23). The milder phenotypes in AQP disruptions in general are surprising, since water is vital for organisms. Therefore, AQPs seem to be not critically essential for the survival of mammals but seem to be involved in the quality of their lives.

The completion of human genome projects has revealed two more aquaporin-like genes, which we have deposited in GenBank under the names of *AQPX1* and *AQPX2* (9). They are renamed *AQP11* and *AQP12* with the approval of the Human Gene Nomenclature Committee. Rat AQP11 (*AQPX1*) is highly expressed in the testis and moderately expressed in the kidney, liver, and brain. On the other hand, rat AQP12 (*AQPX2*) is selectively expressed in the pancreas. They share

similar genome structures with three exons, which are distinct from other AQPs: *AQP0*, *AQP1*, *AQP2*, *AQP4*, *AQP5*, and *AQP6* have four exons; *AQP3*, *AQP7*, *AQP8*, *AQP9*, and *AQP10* have six exons. In humans, *AQP11* is mapped to chromosome 11q14 and *AQP12* to chromosome 2q34-37, to which no diseases have been mapped. Moreover, we were not able to express them functionally in *Xenopus* oocytes. Therefore, their functions and physiological significance remain to be clarified.

Previous AQPs have two highly conserved, short sequences named NPA (asparagine-proline-alanine) boxes. Each one of the NPA boxes has a span of relatively hydrophobic amino acids. They form loops directed into the membrane, which constitute a pore as revealed by three-dimensional structure analyses of AQP1 (14, 20). Interestingly, AQP11 and AQP12 have unique NPA boxes distinct from those of other AQPs, which suggests their unusual pore structures and functions. Several AQPs with these different NPA boxes are present in the GenBank database. They have low homology (~20%) with conventional AQPs. So far, they are found only in multicellular organisms and are absent in monocellular organisms, such as bacteria, yeasts, and protozoans. A yeast (*Saccharomyces cerevisiae*) AQP (*Fps1*) with unusual N and C termini still has conserved NPA boxes and should not be included here (1). In a plant, *Arabidopsis thaliana*, three members have been identified in 35 AQPs. They are named SIP (short membrane intrinsic protein) as a distinct subfamily (12), whose functions and localizations are still unknown. In an insect, *Drosophila melanogaster*, only one member is found in all eight AQPs. In a nematode, *Caenorhabditis elegans*, three NPA members are

* Corresponding author. Mailing address: Department of Molecular Biology Research, Institute of Clinical Investigation, Chiba-East National Hospital, National Hospital Organization, 673 Nitona, Chuou-ku, Chiba 260-8712, Japan. Phone: 81-43-261-5171. Fax: 81-43-268-2613. E-mail: kishiba@nitona.hosp.go.jp.

present in 11 AQPs. Currently, the functions and physiological roles of these AQPs have not been examined. As each AQP has distinct sequences around NPA boxes, each may have a unique function.

In order to get insight into the physiological roles of this new aquaporin, we have disrupted the *AQP11* gene in mice by gene targeting. AQP11-null mice were born normally but died before weaning. The cause of death was advanced renal failure due to polycystic kidneys. The cyst formation was unexpected and preceded by epithelial cell swelling with intracellular vacuolization of the proximal tubule.

MATERIALS AND METHODS

Northern blot analysis. A mouse multiple-tissue Northern blot containing 2 μ g of poly(A)⁺ RNA was obtained (Clontech) and hybridized for 3 h at 68°C in hybridization solution (Express Hyb; Clontech) with randomly primed full-length mouse *AQP11* cDNA (GenBank accession no. AB028148) labeled with [³²P]dCTP. Subsequently, the membrane was washed under high-stringency conditions and developed by radiography as previously reported (7). Total RNAs of mouse tissues were isolated by using a RNeasy kit (QIAGEN), electrophoresed on a 0.8% agarose gel, and transferred to a nylon membrane (Hybond+; Amersham). Northern blotting was conducted as described above.

Production of a polyclonal antibody and immunoblotting. An oligopeptide (TM50) corresponding to the COOH-terminal amino acids of mouse AQP11 (CLPWLHNNQMTNKKE; N-terminal cystine residue was added for conjugation) was synthesized. A rabbit polyclonal antibody to mouse AQP11 (RaTM50b) was raised by using the TM50 peptide conjugated to keyhole limpet hemocyanin (Pierce, Rockford, IL). Affinity purification of the antibody was carried out using SulfoLink coupling gel (Pierce) and yielded an affinity-purified RaTM50b antibody (AffRaTM50b).

The kidneys were quickly removed from the mouse, frozen, and stored at -80°C prior to use. The whole-kidney samples were homogenized in buffer (0.3 M sucrose, 25 mM imidazole, 5 mM EDTA, pH 7.2, containing 5 μ g/ml leupeptin, 5 μ g/ml aprotinin, 5 μ g/ml pepstatin, and 2 mM phenylmethylsulfonyl fluoride) using an Ultra-Turrax T25 homogenizer (IKA Labortechnik, Staufen, Germany) at maximum speed for 10 s. COS7 cells were transiently transfected with pCMVSPORT containing the entire mouse *AQP11* gene, scraped from the dish, and homogenized in phosphate-buffered saline (PBS) containing 5 μ g/ml leupeptin, 5 μ g/ml aprotinin, 5 μ g/ml pepstatin, 5 mM EDTA, and 2 mM phenylmethylsulfonyl fluoride using a glass homogenizer. The protein content of the whole cell was determined using a BCA protein assay kit (Pierce) and bovine serum albumin (BSA) as a standard. These samples were denatured in an equal volume of buffer containing 50 mM Tris-HCl, pH 7.5, 4% sodium dodecyl sulfate (SDS), 300 mM dithiothreitol, and 50% glycerol at 37°C for 30 min, subjected to SDS-polyacrylamide gel electrophoresis, and transferred onto polyvinylidene difluoride membranes by the standard method. Membranes were blocked with 5% nonfat dried milk and 1% BSA in 10 mM Tris-HCl, pH 7.5, containing 150 mM NaCl, 1 mM EDTA, and 0.1% Triton X-100 for 3 h and incubated overnight at 4°C with antibody to AQP11 followed by a horseradish-peroxidase-coupled secondary antibody (P0448 [DAKO, Glostrup, Denmark]; diluted 1:10,000) at room temperature for 3 h. The specificity of AQP11 immunolabeling was verified by preincubating the antibody with the TM50 peptide used as the immunogen. The visualization was performed using ECL plus (Amersham Biosciences Pharmacia, Buckinghamshire, United Kingdom) and Hyperfilm ECL (Amersham Biosciences).

Immunohistochemistry of the kidney. The kidneys were quickly removed from the mouse, cut, and fixed overnight at 4°C with 3% paraformaldehyde in 0.1 M cacodylate buffer, pH 7.4, containing 25 mM CaCl₂. Fixed tissues were immersed in 20% sucrose-0.1 M cacodylate buffer, pH 7.4, embedded in Tissue-Tek optimal cutting temperature (OCT) compound, and frozen in liquid nitrogen. Cryostat sections 7 to 8 μ m thick were mounted on silane-coated glass slides (Matsunami, Osaka, Japan) and air dried. To retrieve antigens, sections were placed in 20 mM Tris buffer, pH 9.0, and heated in an autoclave at 100°C for 10 min (22). Endogenous peroxidase activity was blocked by 0.5% H₂O₂ in methanol for 30 min at room temperature. Sections were blocked with PBS containing 5% normal goat serum and then incubated overnight at 4°C with the antibody to AQP11 diluted in PBS containing 5% normal goat serum. After the sections were rinsed in PBS, they were incubated with a horseradish peroxidase-coupled goat antibody to rabbit immunoglobulins using the Histofine kit (catalog no. 414181; Nichirei, Tokyo, Japan). The specificity of AQP11 immunostaining was

verified by (i) preincubating the antibody with the TM50 peptide used as the immunogen and (ii) incubating the sections with PBS containing 5% normal goat serum without the antibody to AQP11. Diaminobenzidine (DAB) reaction was performed using liquid DAB+ substrate chromogen system (K3467; DAKO). After the sections were rinsed in water, they were mounted with aqueous mounting medium (catalog no. 415131; Nichirei). Immunolabeled sections were examined with an Eclipse E800 light microscope (Nikon, Tokyo, Japan). Micrographs were taken with a DP-50 digital camera (Olympus, Tokyo, Japan) and processed with Adobe Photoshop software (Adobe Systems, San Jose, CA).

To identify subcellular organelles, the cryostat sections were similarly stained with anti-KDEL monoclonal antibody (Stressgen Biotechnologies, Victoria, British Columbia, Canada) (diluted 1:400) for endoplasmic reticulum (ER), with anti-mannose-6-phosphate receptor (Affinity BioReagents, Golden, CO) for endosomes, or with anti-adaptin-gamma (Transduction Laboratories, Lexington, KY) for Golgi complexes.

Expression of GFP- or V5-tagged AQP11 in cultured cells. The green fluorescent protein (GFP)- or V5-tagged AQP11 construct (GFP-AQP11 or AQP11-V5) was made by subcloning mouse *AQP11* cDNA in frame into the pEGFP-C1 (Clontech) or pcDNA-DEST40 (Invitrogen) vector, respectively. The pDsRed2-ER vector (Clontech) was used for fluorescent labeling of ER. The CHO-K1 cells (obtained from the American Type Culture Collection) (CCL-61) were maintained on glass coverslips in Ham's F-12 medium (Invitrogen) containing 3.5 mM NaHCO₃, 100 U/ml penicillin, 100 μ g/ml streptomycin, and 20% fetal bovine serum in a humidified atmosphere of 95% air and 5% CO₂ at 37°C. The cells were transfected at 50 to 60% confluence using Lipofectamine 2000 (Invitrogen) according to the manufacturer's instructions. The cultured cells were observed 1 day posttransfection with an MRC-600 (MRC-600) or a FV-300 (Olympus) confocal microscope. To detect V5, the fixed cells were immunolabeled with a FITC-labeled anti-V5 antibody (catalog no. 46-0308; Invitrogen) (diluted 1:250) after the cells were mildly permeabilized with 0.1% saponin.

Generation of *AQP11* knockout mice. *AQP11* knockout mice were generated on a commercial basis by Lexicon Genetics, Inc. (The Woodlands, TX). The *AQP11* gene was cloned from a 129/SvEvBrd genomic library and used to construct a targeting vector containing the neomycin resistance gene flanked by two *AQP11* genomic fragments spanning the regions of partial exon 2, total intron 2, exon 3, and intron 3. The shorter fragment of the target construct was 3 kb long from intron 1 and was upstream of exon 2. The longer fragment was 3.7 kb long and was downstream of intron 3 (Fig. 1). The targeted allele contained a deletion of *AQP11* gene exons 2 and 3, which corresponded to downstream of the second NPA box of *AQP11*. Lex-1 embryonic stem cells (derived from the 129/SvEvBrd strain) were transfected with the targeting vector. G418-resistant colonies were analyzed by PCR to identify homologous recombinants. Homologous recombinants were confirmed by Southern blot analysis for wild-type 4.7-kb and *neo*-disrupted 8.1-kb *StuI* fragments using the 5'-end probe shown in Fig. 1. Two correctly targeted embryonic stem cell clones were separately injected into 129/SvEvBrd blastocysts to generate chimeric mice, which were bred with 129/SvEvBrd mice to obtain heterozygous offspring. Heterozygous founder mice containing the disrupted *AQP11* gene in the germ line were intercrossed to produce homozygous *AQP11* knockout mice. Mouse genotyping was performed with genomic DNA isolated from tail tips using a genomic DNA isolation kit (QIAGEN). The wild-type *AQP11* allele was identified by PCR using primers 5'-GTTTTTAAAGCCATAACCTT-3' and 5'-GCCCTCATTTCTTAACCTT G-3', which amplified a 402-bp product. The knockout allele was identified by PCR using primers 5'-CAGAATTTCTTGGTCCTGCC-3' and 5'-GCAGCGC ATCGCCTTCTATC-3', which amplified a 262-bp product containing a fragment of the neomycin resistance cassette. The PCR protocol consisted of 35 cycles of denaturation at 96°C for 17 s, annealing at 56°C for 30 s, and extension at 72°C for 45 s.

Light microscopy and electron microscopy. For light microscopy, the kidneys were fixed in formaldehyde and embedded in paraffin. The sections were stained with hematoxylin and eosin.

For transmission electron microscopy, the mice were perfused from the left ventricle with 2.5% glutaraldehyde-2% paraformaldehyde-0.1 M sodium phosphate buffer, pH 7.4. The kidneys were removed and further fixed in the same solution at 4°C overnight. They were then osmicated and embedded in Epon 812. The ultrathin sections were stained with uranyl acetate and lead citrate and finally examined with a JEOL JEM-1010 electron microscope (Tokyo, Japan).

Primary culture of proximal tubular cells from the kidney. Cells were cultured from collagenase-digested fragments of proximal tubules from 7- to 10-day-old mice using a modified version of established methods (5, 18). Briefly, cortices were minced and incubated with 0.5 mg/ml collagenase and 0.5 mg/ml soybean trypsin inhibitor in Hanks' balanced salt solution for 30 min. After large undigested fragments were removed by gravity, the suspension was mixed with an

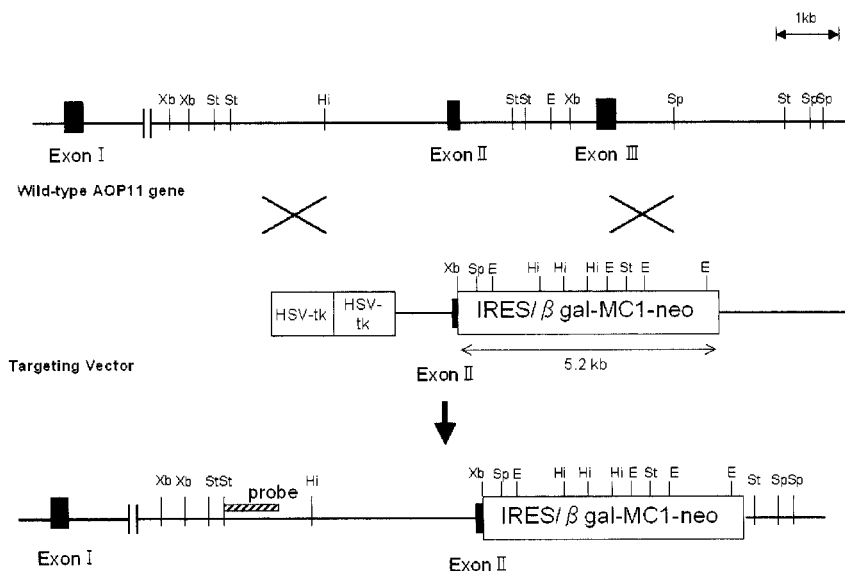


FIG. 1. Schematic representation of the targeting strategy for AQP11-null mice. Homologous recombination results in replacement of the indicated segment of the *AQP11* gene by a neomycin selection cassette. A herpes simplex virus thymidine kinase cassette (HSV-tk) was used for negative selection. The position of the probe used for Southern blot analysis is shown in the bottom map. Abbreviations: Xb, XbaI; St, StuI; Hi, Hinc-II; E, EcoRI; Sp, SpeI; IRES, internal ribosome entry site; β gal, β -galactosidase.

equal volume of 10% fetal bovine serum in Hanks' balanced salt solution and then centrifuged for 7 min at $50 \times g$ at 4°C . The pellets containing cortical tubules were washed with ice-cold Hanks' balanced salt solution, centrifuged for 2 min at $50 \times g$ at 4°C , washed again with Dulbecco modified Eagle medium/Ham's F-12 medium (DMEM/F-12), centrifuged, and resuspended in DMEM/F-12. Cortical tubules were purified by gradient centrifugation in a 40% Percoll-60% DMEM/F-12 at $36,000 \times g$ for 20 min at 4°C . The band containing renal proximal tubules was collected and washed twice with DMEM/F-12, and the final pellet was resuspended in DMEM/F-12. Cells were plated on 18-mm-diameter round coverslips. The medium used to grow cells was a serum-free mixture of DMEM/F-12 containing 2 mM glutamine, 15 mM HEPES, 5 $\mu\text{g}/\text{ml}$ transferrin, 5 $\mu\text{g}/\text{ml}$ insulin, and 50 mM hydrocortisone. Measurements of pH and $[\text{Cl}^-]$ were done after 4 to 6 days of culture when the cells were nearly confluent.

The proximal tubular origins of wild-type and AQP11-null cells were confirmed by detecting *AQP1* mRNA by reverse transcription-PCR. Total RNAs were isolated from the cultured cells using RNeasy Mini kit (QIAGEN). Reverse transcription-PCR was performed using mRNA Selective PCR kit version 1.1' (Takara-BIO, Japan) following the manufacturer's instruction. Deoxynucleoside triphosphate (dNTP) analogs are used in this kit. The dNTP analogs are incorporated into synthesizing cDNA to permit the annealing temperature to be so low that genomic DNA cannot anneal to primers to prevent the PCR on genomic DNA. The primers for AQP1 were 5'-TCGTCTTCATCAGCATTGGTT-3' and 5'-CATGCGGTCTGTGAAGTCG-3'. The cDNAs were synthesized at 42°C for 30 min. Thirty PCR cycles were done; one PCR cycle consisted of 85°C for 1 min, 45°C for 1 min, and 72°C for 1 min. Both denaturing and annealing temperatures were lower due to dNTP analogs to avoid the amplification of genomic DNA.

Endosome labeling and kinetics of endosomal $[\text{Cl}^-]$ and pH. Fluorescently labeled Tf (transferrin) and $\alpha_2\text{M}$ (α_2 -macroglobulin) were synthesized as described previously (5, 19). Cells were incubated in PBS for 15 min at 37°C before experiments. Surface labeling was done by incubation with Cl or pH sensors (300 nM for Tf; 100 nM for $\alpha_2\text{M}$) for 20 min in PBS (containing 1 mM CaCl_2 and MgCl_2) at 4°C . Coverslips were then washed twice with ice-cold PBS and transferred to a precooled perfusion chamber containing ice-cold perfusate. Sets of BAC (10,10'-bis[$-\text{carboxypropyl}$]-9,9'-biacridium dinitrate) and TMR (5- [and 6]-carboxytetramethylrhodamine) images (for Cl) or FITC (fluorescein isothiocyanate) and TMR images (for pH) were acquired at specified time points after rapid warming by perfusion at 37°C (4, 5).

Animal procedures and serum analysis. All the animal procedures were approved by the Committee on Research Animal Care of Jichi Medical School. Blood was drawn from the vena cava under light ether anesthesia. Blood chemistry was determined by a clinical chemistry laboratory (SRL, Hachioji, Tokyo).

Statistical analysis. Data are given as means \pm standard errors (SE). Statistical significance was determined by Fisher's protected least significant difference (PLSD) test, and P values less than 0.01 were considered statistically significant.

RESULTS

AQP11 expression in the kidney. Northern blot analysis of mouse tissues revealed *AQP11* mRNA expression in the testis, kidney, and liver (Fig. 2). Much weaker expression was observed in the heart, brain, and muscle. The most prominent

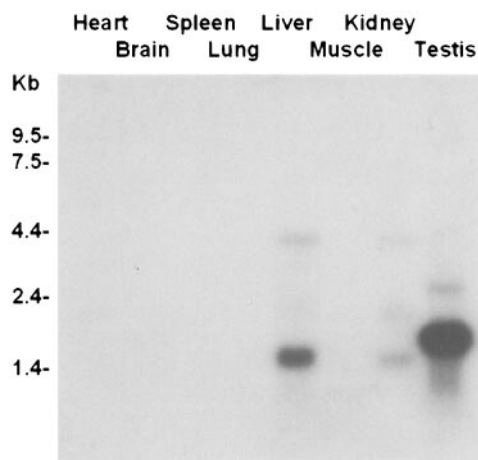


FIG. 2. A multiple-tissue Northern blot showing AQP11 transcript distribution in the mouse. Two micrograms of poly(A)⁺ RNA was loaded in each lane. The probe was synthesized from the entire length of mouse *AQP11* cDNA (GenBank accession no. AB028148). Three transcripts were detected in the testis, liver, and kidney. The transcripts from the testis were larger. After longer exposure, the transcript was also detected in the heart, brain, and muscle (data not shown).

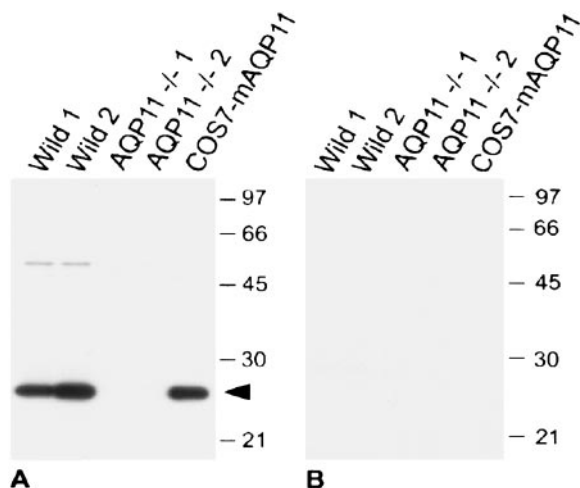


FIG. 3. Immunoblotting of kidneys with the antibody to AQP11. (A) Ten micrograms of whole-kidney homogenates from two wild-type mice and two AQP11^{-/-} mice and 10 ng of homogenate from COS7 cells transfected with mouse AQP11 (COS7-mAQP11) were subjected to immunoblotting with an affinity-purified rabbit antibody to AQP11 (AffRaTM50b, 40 ng/ml). (B) The rabbit antibody to AQP11 was preincubated with the antigen peptide (2 μg/ml). A dense band around 26 kDa was obtained in wild-type mice as well as mouse AQP11-transfected COS7 cells (arrowhead in panel A). The bands completely disappeared in the presence of antigen peptide TM50 in panel B. The positions of molecular size markers (in kilodaltons) are shown to the right of the gels.

expression was observed in the testis. The expression pattern was similar to that in the rat (9). Three sizes of the transcript are most likely due to the usage of different polyadenylation sites. Interestingly, the sizes of the bands in the testis were larger than those from other tissues. This may be due to the different lengths of the poly(A) tails.

We then examined AQP11 localization in the kidney. We raised a polyclonal antibody against the C-terminal polypeptides of mouse AQP11. Western blotting of the membrane fraction of mouse kidneys revealed that the size of AQP11 was ~26 kDa (Fig. 3A), while the calculated size is 30 kDa. The smaller size may indicate secondary protein modifications or an aberrant movement in SDS-polyacrylamide gel electrophoresis. A weak larger band may indicate AQP11 dimer. In addition, analysis of COS7 cell membranes expressing recombinant mouse AQP11 confirmed the specific immunoreactivity of the antibody. Preabsorption of the antibody with the immunizing peptides abolished all staining (Fig. 3B).

The immunohistochemistry of the 8-day-old mouse kidney revealed that AQP11 was seen in the cortex, where it was present selectively in the proximal tubule (Fig. 4A). At a higher magnification, AQP11 was localized in the cytoplasm, especially around the nucleus, and absent at the brush border membrane (Fig. 4D). To check the specificity of staining, the following control experiments were carried out. When we replaced the antibody with antibody preincubated with the anti-

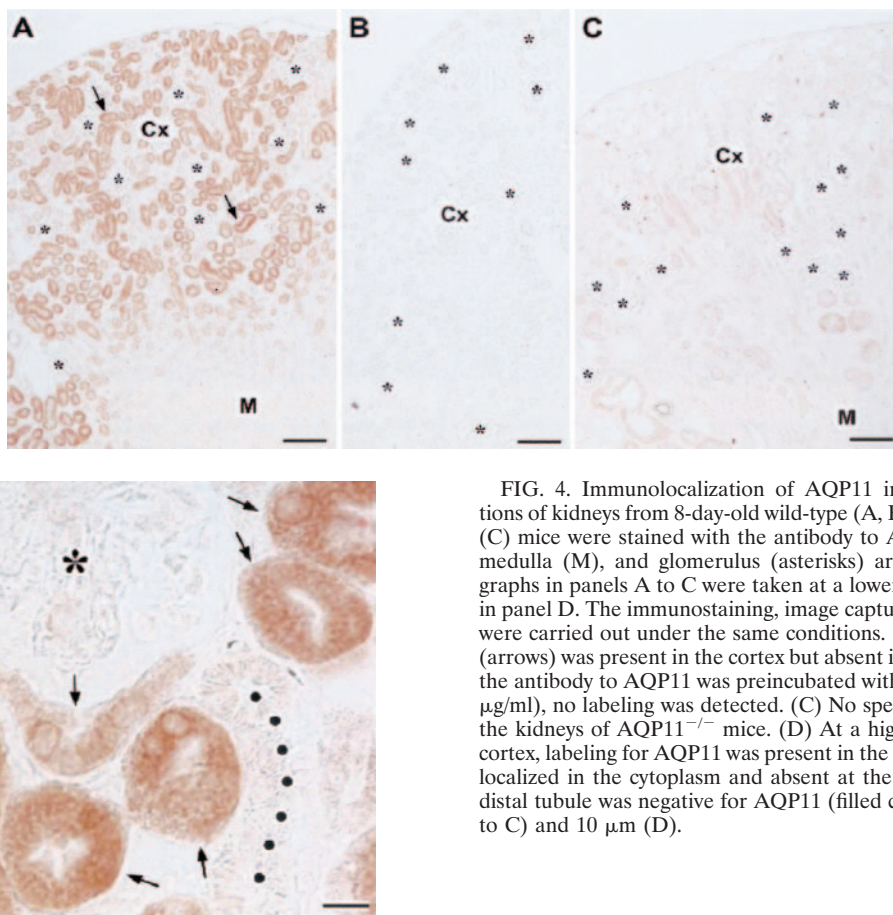


FIG. 4. Immunolocalization of AQP11 in kidneys. Cryostat sections of kidneys from 8-day-old wild-type (A, B, and D) and AQP11^{-/-} (C) mice were stained with the antibody to AQP11. The cortex (Cx), medulla (M), and glomerulus (asterisks) are indicated. The micrographs in panels A to C were taken at a lower magnification than that in panel D. The immunostaining, image capture, and image processing were carried out under the same conditions. (A) Labeling for AQP11 (arrows) was present in the cortex but absent in the medulla. (B) When the antibody to AQP11 was preincubated with the antigen peptide (10 μg/ml), no labeling was detected. (C) No specific labeling was seen in the kidneys of AQP11^{-/-} mice. (D) At a higher magnification of the cortex, labeling for AQP11 was present in the proximal tubule (arrows) localized in the cytoplasm and absent at the plasma membrane. The distal tubule was negative for AQP11 (filled circles). Bars, 100 μm (A to C) and 10 μm (D).

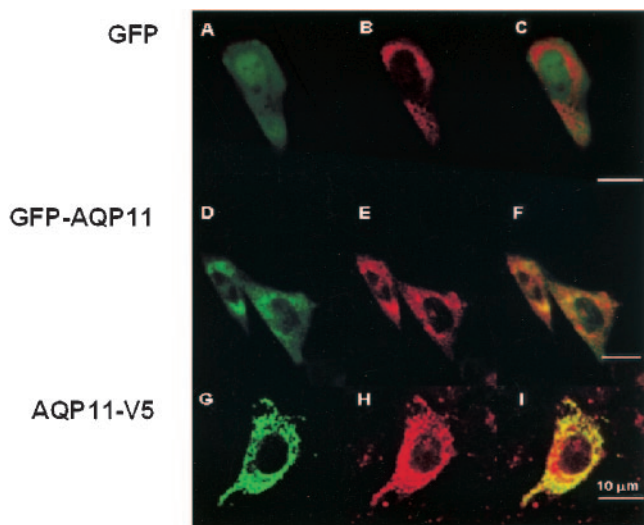


FIG. 5. Subcellular localization of transfected AQP11. CHO-K1 cells were cotransfected with pDsRed2-ER (an ER marker; red) (B, E, and H) together with the expression plasmid coding for GFP (A to C), GFP-AQP11 (D to F), or AQP11-V5 (G to I). Colocalization was visualized by image overlay (C, F, and I) (yellow). GFP was expressed in the cytoplasm but was not colocalized with the ER marker (still red in panel C). On the other hand, GFP-AQP11 or AQP11-V5 was colocalized with the ER marker (yellow in panels F and I). Bars, 10 μ m.

gen peptide, no labeling was detected (Fig. 4B). Moreover, when we replaced the antibody with PBS containing 5% normal goat serum, no labeling was detected (not shown). These results confirmed the specificity of immunohistochemical staining. Thus, AQP11 is an intracellular protein similar to AQP6 and AQP8 (3, 24).

Subcellular localization of transfected AQP11. In order to examine the function of AQP11, we tried to express AQP11 in exogenous systems. For the visualization of AQP11 protein, the GFP gene or V5 was introduced at the N terminus or C terminus, respectively, of AQP11 in a plasmid construct to be translated as a fusion protein, GFP-AQP11 or AQP11-V5. Each plasmid (GFP, GFP-AQP11, or AQP11-V5), together with an ER marker (pDsRed2-ER vector), was transiently transfected into CHO-K1 cells, and the localizations of expressed proteins were analyzed by confocal microscopy. GFP alone was diffusely observed in the cytoplasm (Fig. 5A), which was not colocalized with the ER marker (Fig. 5C). In contrast, the localizations of GFP-AQP11 and AQP11-V5 overlapped with that of the ER marker (Fig. 5F and I). GFP-AQP11 and AQP11-V5 were absent at the plasma membrane (Fig. 5D and G). Similarly, exogenous AQP11 was expressed intracellularly and not targeted to the plasma membrane in *Xenopus* oocytes (data not shown). Since AQP11 was not expressed at the plasma membrane in cultured cells and *Xenopus* oocytes, conventional methods of measuring the transport of water and small solutes could not be used to clarify the function of AQP11.

AQP11 knockout mice. As the function of AQP11 was difficult to study, we generated mice deficient of AQP11 through gene targeting in embryonic stem cells (Fig. 1). Two independent embryonic stem clones with a desired homologous recombination were separately injected into 129/SvEvBrd blastocysts.

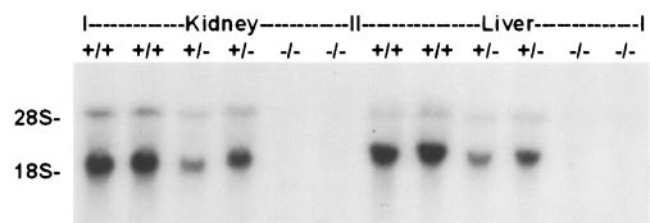


FIG. 6. Northern blot analysis of total RNA (10 μ g in each lane) from kidneys and livers using the full-length mouse *AQP11* cDNA as a probe. The bands of the heterozygous mouse (+/-) were weaker than those of the wild-type mouse (+/+), and there were no bands in the homozygous mouse (-/-).

Two lines of chimeric mice were bred independently, and their offspring were analyzed for phenotype abnormalities. As both lines of *AQP11*^{-/-} mice showed similar phenotypes, data were reported together. The correct targeting was confirmed by Southern blot analysis using a 5'-end probe. To demonstrate the successful knockout of *AQP11*, we analyzed the expression of *AQP11* mRNA and protein in *AQP11*^{-/-} mice. The expression of *AQP11* mRNA in the kidney and liver is shown in Fig. 6. *AQP11* mRNA expression was reduced in *AQP11*^{+/-} mice and absent in *AQP11*^{-/-} mice. The *AQP11* knockout was further analyzed at the protein level. Equal amounts of whole-kidney homogenates from two wild-type and *AQP11*^{-/-} 8-day-old mice were analyzed by Western blotting. The band was not detected in *AQP11*^{-/-} mice (Fig. 3B). Similarly, immunohistochemistry revealed no staining in the kidney of *AQP11*^{-/-} mice (Fig. 4C). These results confirmed that AQP11 protein was not expressed in *AQP11*^{-/-} mice.

AQP11^{-/-} mice were born normally at the expected Mendelian frequency and were indistinguishable from their *AQP11*^{+/+} and *AQP11*^{+/-} littermates at birth. However, by the second week, a failure to thrive became apparent as shown in a growth curve (Fig. 7A). The *AQP11*^{-/-} mice began dying after 15 days, and only 15% survived until day 60 as shown in a survival curve (Fig. 7B). The cause of death was advanced renal failure as revealed by the blood chemistry (Fig. 7C). The kidneys were large and pale with rough texture occupying the whole abdominal cavity in *AQP11*^{-/-} mice (Fig. 8A). The kidneys were anemic and polycystic (Fig. 8B). There was no difference in *AQP11*^{+/+} and *AQP11*^{+/-} mice in survival and growth rates as well as the morphology and function of the kidney.

Histological examination of the kidney from a 1-month-old mouse revealed the advanced stage of polycystic kidney with cysts occupying the cortex (Fig. 9A). The cysts were absent in the medulla, which suggests that cysts originated from the proximal tubule. Remarkably, the cyst epithelia had vacuoles in the cytoplasm (Fig. 9B). We then analyzed the time course of the cyst development after birth. The cysts were absent at birth, but some of the tubules were swollen due to large vacuoles (Fig. 9C). In 1-week-old mice, these swollen tubules occupied the whole cortex. The swelling of the tubular epithelia progressed to obliterate the lumen (Fig. 9D). Vacuoles occupied the whole cytoplasm, appearing like spider webs. Glomeruli appeared normal. In 3-week-old mice, these tubules opened to develop into small cysts, whose epithelia still had multiple small vacuoles. Finally, larger cysts developed in 1-month-old

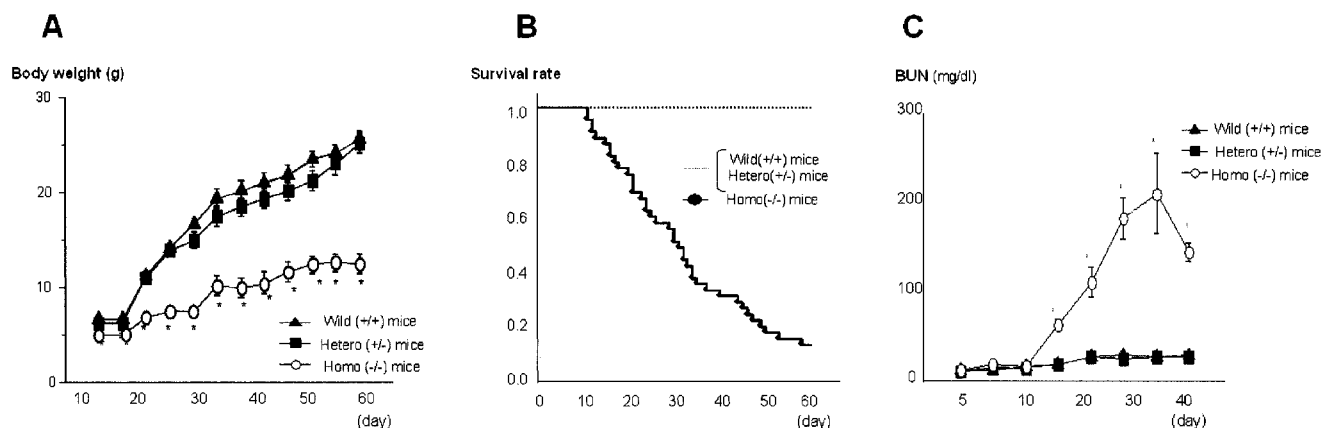


FIG. 7. (A) Change in body weight after birth. The wild-type mice (+/+) and the heterozygous mice (+/-) grew progressively, while the homozygous mice (-/-) had retarded growth. Values are means ± SE (error bars) of 90 mice. (B) Survival rate after birth. The wild-type mice (+/+) and the heterozygous mice (+/-) survived, but the homozygous mice (-/-) began to die after 15 days (*n* = 90). (C) Blood urea nitrogen (BUN). BUN, an indicator of renal dysfunction, increased progressively after 10 days in the homozygous mice (-/-). Values are means ± SE (error bars) of 30 mice. Values that are statistically significantly different from the values for wild-type mice by Fisher's PLSD test are indicated (*, *P* < 0.01).

mice (Fig. 9A). Therefore, vacuoles were observed throughout the proximal tubule development in AQP11^{-/-} mice. These vacuoles appeared empty and contained no oil red-positive substances, even in frozen sections, to prevent the loss of contents into solvents (data not shown). The origin of the vacuoles was examined by organelle-specific antibodies. They were strongly stained by an anti-KDEL antibody suggesting their ER origin (Fig. 10A). No staining with anti-adaptin-gamma antibodies (Fig. 10B) and the minimum staining with anti-mannose-6-phosphate (Fig. 10C) indicated that Golgi and endosomal components were small.

Next, we analyzed the kidney by electron microscopy. As shown in Fig. 11A, the brush border was detected in a vacuolized cell, indicating that it was a proximal tubular cell. Large vacuoles were connected to the outer membrane of the nuclear envelope, suggesting that they came from ER (Fig. 11B). In fact, ribosomes were observed on the cytoplasmic side of vac-

uolar membrane (Fig. 11C). There were no remarkable changes in the nucleus, Golgi apparatus, and mitochondria (Fig. 11C), suggesting the absence of major cell damage. The vacuoles appeared to be empty, without any electron-dense material.

Although AQP11 is expressed widely, the other organs in AQP11^{-/-} mice appeared normal at the macroscopic level. However, histological examination revealed similar vacuolization in hepatocytes limited to the portal area without any fibrosis or cyst formation. Since the life span of AQP11^{-/-} mice is limited by the kidney disease, the liver phenotype may be premature. Similarly, their death before testis maturation and uremia made the histological analysis of the testis inconclusive.

Primary culture and endosomal [Cl⁻] and pH. As the swelling of intracellular organelles does not seem to be caused by cell damage, we then examined the function of intracellular vesicles. We studied the function of endosomes. For in vitro

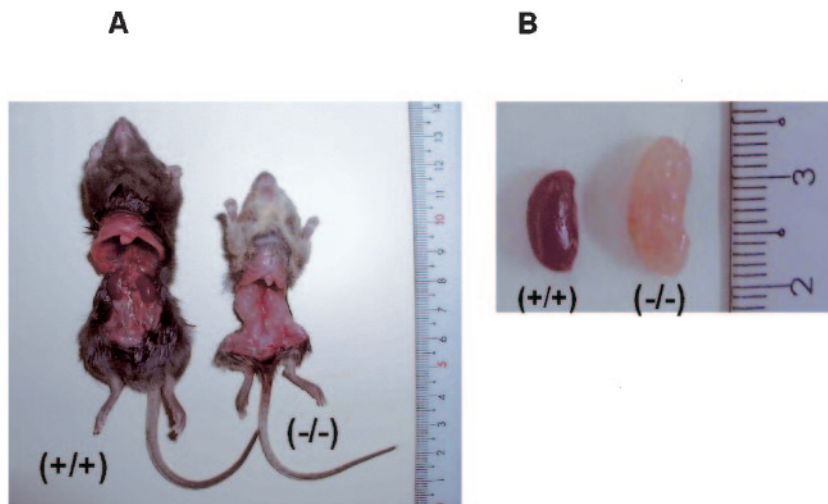


FIG. 8. Gross anatomy of AQP11-null mice. (A) Photograph showing a 30-day-old wild-type mouse (+/+) on the left and a 30-day-old AQP11-null mouse (-/-) on the right. The AQP11-null mouse was smaller than the wild-type mouse. Polycystic kidneys occupied the entire abdominal cavity in the AQP11-null mouse. (B) Photograph showing the larger and paler kidney of the AQP11-null mouse.

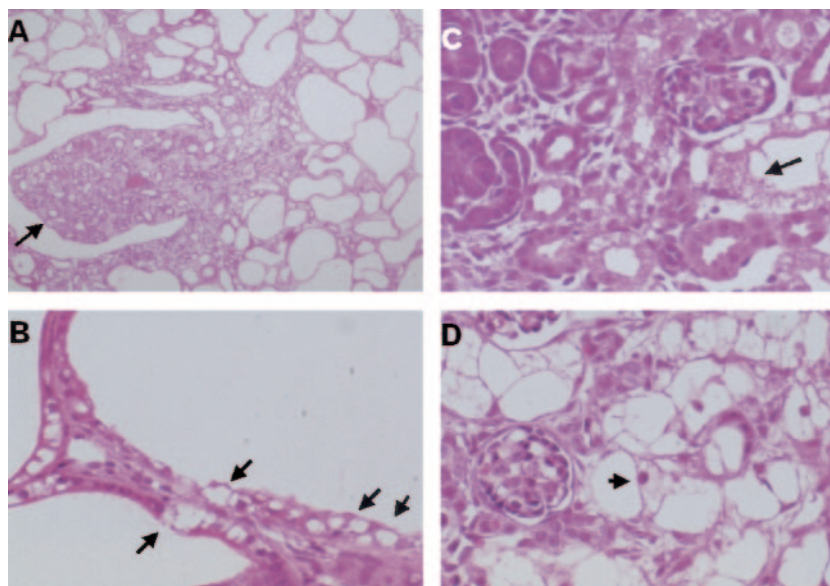


FIG. 9. Histological examination of the kidney from AQP11-null mice by light microscopy and hematoxylin and eosin staining. (A) Kidney section from a 1-month-old mouse. Note multiple cysts occupying the entire cortex with an intact papilla (arrow). (B) High-magnification view of kidney section. The epithelia of the cysts contained many vacuoles (arrows). (C) Kidney section from a newborn mouse. Some tubular cells in the deep cortex were swollen and vacuolized (arrow). (D) Kidney section from a 2-week-old mouse. Additional swollen proximal tubular cells were observed. The nuclei were not flattened despite advanced vacuolization (arrow).

measurement, the primary cultured cells of the proximal tubule were obtained from 1-week-old mice, in which most of the proximal tubules of AQP11-null mice were swollen (Fig. 9D). The appearance of the cultured cells was similar in AQP11^{+/+} and AQP11^{-/-} mice by light microscopy (Fig. 12). This standard procedure for the primary culture of proximal tubules previously revealed CIC-5 expression with immunohistochemistry (5). Their proximal tubular origins were further confirmed by the expression of AQP1 (data not shown). The disappearance of vacuoles in AQP11^{-/-} mice is intriguing and may be caused by the absence of solute flux in the cultured condition.

We then measured endosomal [Cl⁻] and pH as previously conducted (4, 5). Immediately after warming to 37°C, endoso-

mal pH decreased, which is probably due to the activation of the H pump. The summaries of the kinetics of endosomal acidification show that the rate of pH reduction was slower in AQP11^{-/-} mice than in AQP11^{+/+} mice for both early (Fig. 13A) and late endosomes (Fig. 13B). However, the rate of [Cl⁻] increase was not different (Fig. 13). Therefore, the cultured proximal tubular cells of AQP11^{-/-} mice had a defect in endosomal pH regulation with normal [Cl⁻] homeostasis.

DISCUSSION

Unlike other AQPs, AQP11 has unusual NPA boxes, which may form a unique pore allowing some substances to perme-

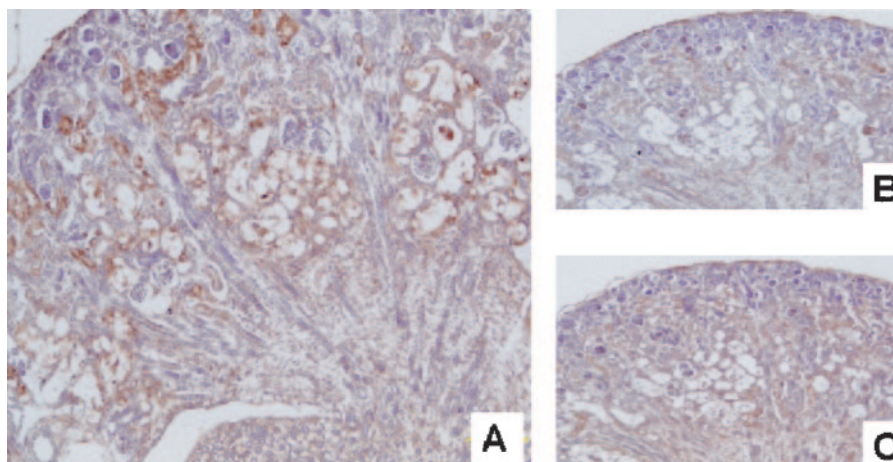


FIG. 10. Immunohistochemistry of kidneys from a 1-week-old AQP11-null mouse. (A) Anti-KDEL staining as an ER marker. Vacuolized proximal tubules were evident in the deep cortex. The strong staining of these vacuoles indicates the ER origin of the vacuoles. (B) Anti-adaptin-gamma, a Golgi marker, failed to stain these vacuoles. (C) Anti-mannose-6-phosphate, an endosome marker, weakly stained these vacuoles.

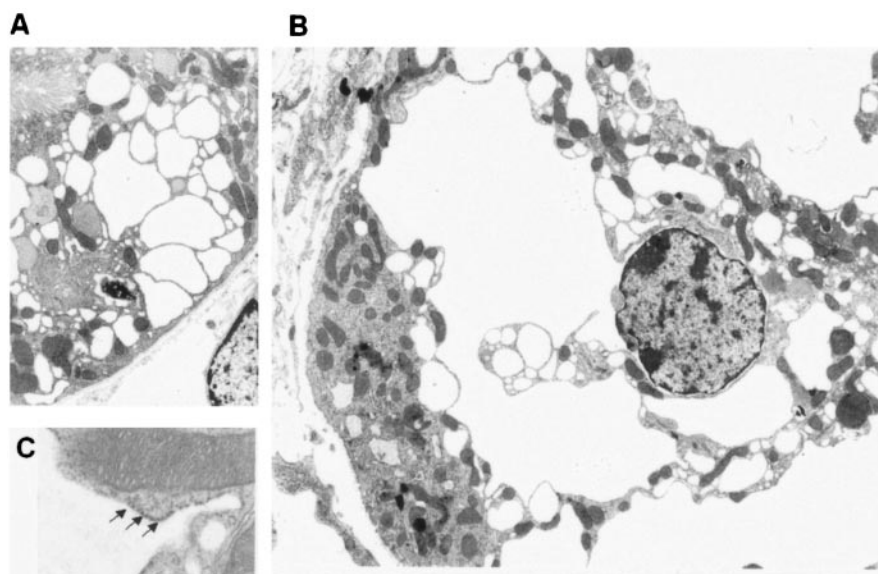


FIG. 11. Electron micrograph of a kidney section from a 1-week-old AQP11-null mouse. (A) At low magnification, multiple vacuoles were detected in the cytoplasm of proximal tubular cells with intact brush border membrane. (B) Swollen intracellular vacuoles were connected to nuclear membranes, suggesting that they originated from the ER. There were no remarkable changes in the nucleus. (C) At high magnification, ribosomes (arrows) were attached to the vacuole membrane. The upper half shows a normal mitochondrion with well-organized cristae.

ate. However, its function is difficult to study, because it did not reach the plasma membrane when expressed in cultured cells or *Xenopus* oocytes. Similarly, the immunohistochemical study revealed that it was localized in the cytoplasm of kidney proximal tubules. Therefore, AQP11 is similar to AQP6 and AQP8 in the cellular localization (3, 24). Interestingly, both AQP6 and AQP8 are targeted aberrantly to the plasma membrane in *Xenopus* oocytes to facilitate functional studies. This difference may be due to the different localization of subcellular compartments. The presence of a putative ER localization signal (-NKKE) similar to a known ER localization signal (-KKXX) at the C terminus of AQP11, which is absent in AQP6 and AQP8, may retain AQP11 in ER and make it difficult to be aberrantly targeted to the plasma membrane in *Xenopus* oocytes. Further mutagenesis studies are necessary to document the importance of this signal for the targeting of AQP11.

Luckily, some mutants may reach the plasma membrane and thus enable functional studies.

In the present study we have shown two principal abnormalities of AQP11-null mice: vacuolization and cyst formation of the proximal tubule. Before generating AQP11-null mice, we thought that redundant expression of other AQPs in the proximal tubule would make it difficult to obtain a distinct phenotype of AQP11-null mice. AQP1 is expressed at the apical and basolateral membranes of the proximal tubule (15). AQP7 is also expressed at the apical membrane of the proximal tubule (10). Moreover, AQP8 is expressed intracellularly in the proximal tubule (3). Despite these redundancies, AQP11-null mice had growth retardation and progressively died before weaning. The cause of death was advanced renal failure.

The birth ratio by crossing AQP11^{+/-} mice followed Mendel's law, suggesting the absence of embryonic fatality. In fact, cysts were absent in the kidneys of newborn mice. Cysts first appeared after 3 weeks when functional renal failure was evident. Remarkably, the cyst epithelia contained vacuoles in the cytoplasm. Such vacuoles had already been observed at birth. The dysfunction of AQP11 will be a direct cause of vacuole formation, because vacuoles were limited to the proximal tubule, in which AQP11 is expressed. As vacuolization precedes the cyst formation, cysts may be caused by the vacuolization. Such precystic abnormalities have not been observed or carefully examined in other cystic kidney diseases. Cysts are usually formed abruptly from renal tubules in polycystic kidney diseases (6). Therefore, the precystic vacuolization in our model is novel, and analysis of its cause may provide an insight into the mechanism for cyst formation and be an important clue to clarify the function of AQP11.

How does vacuolization take place when AQP11 is disrupted? As the intracellular organelles, including mitochon-

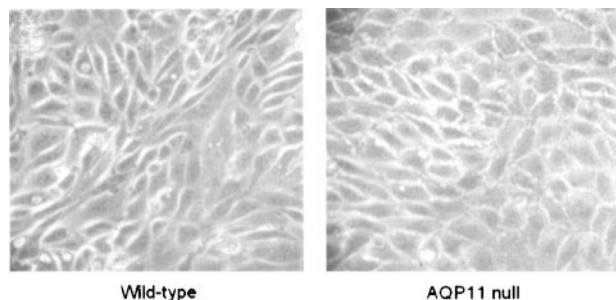


FIG. 12. Phase-contrast light micrographs of proximal tubular cells in primary culture from wild-type and AQP11-null mice. The primary cultured cells of the proximal tubule were obtained from 1-week-old mice. The cells were nearly confluent after 4 to 6 days of culture. There was no difference in the appearance of the cells.

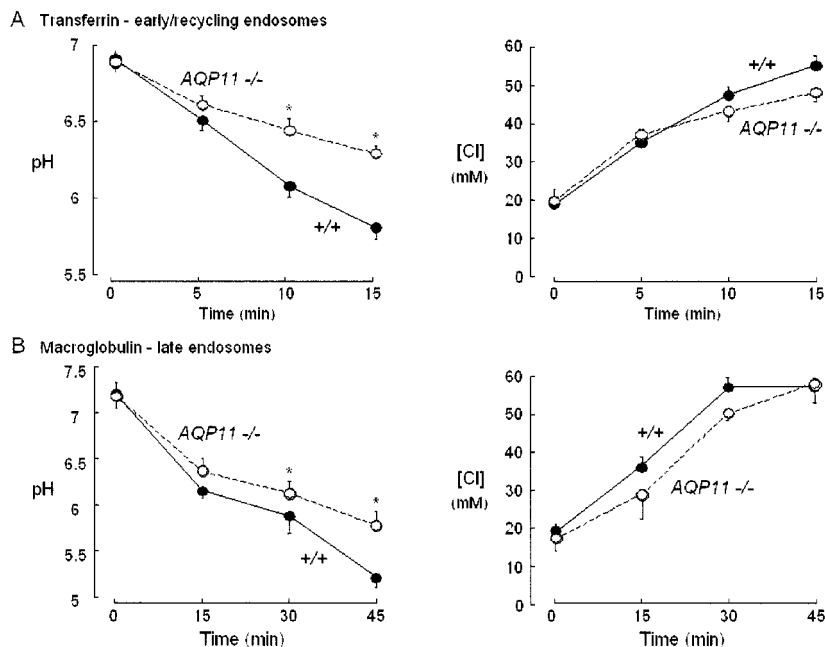


FIG. 13. Kinetics of endosomal pH and [Cl] in Tf (transferrin)- and α_2 M(α_2 -macroglobulin)-labeled endosomes in proximal tubular cells from wild-type (+/+) and AQP11-null (*AQP11* -/-) mice. The time course of endosomal pH and [Cl] at 37°C after labeling at 4°C with FITC- or BAC-dextran-Tf-TMR (A) and FITC- or BAC-dextran- α_2 M-TMR (B) is shown. The proximal tubular cells from wild-type mice (closed circles) and AQP11-null mice (open circles) (mean \pm SE, 7 to 10 imaging sets from two or three mice) were used.

dria, nuclei, and Golgi apparatus, appeared normal, vacuolization does not seem to be caused by general cell damage. The vacuoles are reminiscent of those induced by abnormal protein aggregates in neuronal cells. Certain neurodegenerative disorders, such as Huntington's disease, involve accompanying vacuolization of neural cells. The disruption of electrical and/or electrolyte homeostasis of intracellular vesicles may lead to the dysfunction of the vesicle-localized enzymes, resulting in the accumulation of unprocessed and abnormal proteins inside the vesicles. Such proteins will osmotically swell the vesicles. We examined endosomes as an intracellular vesicular environment. Since AQP6 has been reported to function as an anion channel (24) and Cl is the principal ion in most cells responsible for shunting the interior-positive endosomal potential produced by active H entry (19), we measured endosomal Cl concentration as well as pH. Previously, similar studies were conducted in primary cultured hepatocytes of CIC3-null mice, in which we successfully showed abnormal endosomal pH regulation caused by the disruption of chloride channel function (4). More recently, we also reported a similar abnormality in primary cultured proximal tubular cells of CIC-5-null mice (5). In the present study, we also showed that primary cultured proximal tubules of AQP11-null mice had impaired endosomal acidification. However, endosomal Cl concentration was similar to that of wild-type mice. The results suggest that AQP11 does not function as a main anion channel at endosomes of the proximal tubule, where CIC-5 should be a major anion channel (5, 17). Because the determinants of endosomal acidification are complex, it is difficult to speculate the cause of endosomal acidification defect in AQP11-null mice. AQP11 may modulate the activities of H-pump and/or Na-H exchanger or the buffering capacity of endosomes. Whatever the mechanism, the

endosomal acidification defect may lead to the accumulation of endocytosed substances, which osmotically swell the endosomes.

As CIC-5 is a major endosomal anion channel of the proximal tubule, its disruption has been shown to lead to endosomal acidification defect (5). In fact, the kidneys of CIC-5 null mice have impaired endocytosis but do not show vacuolization or cysts (17). Therefore, an endosomal acidification defect alone will not explain the kidney phenotype of AQP11-null mice. As shown in Fig. 10, most of the vacuoles came from ER. If a similar pH abnormality in other intracellular compartments is present in AQP11-null mice, the subsequent enzyme dysfunction will result in abnormal folding of proteins to be accumulated in the cell, leading to swollen compartments, particularly ER as revealed by electron microscopy in Fig. 11. Interestingly, mutations in genes encoding enzymes in the ER are found to be responsible for autosomal dominant polycystic liver diseases (2). The dysfunction of ER will be a new mechanism for cyst formation in the kidney, too. Further works are necessary to clarify the mechanism of vacuolization and its correlation with cyst formation.

Currently, no human kidney diseases similar to kidney disease in AQP11-null mice have been reported. The closest diseases are autosomal recessive polycystic kidney disease and nephrophthosis with polycystic kidneys. However, their cysts also originate from the collecting duct, while the cysts of AQP11-null mice are limited to the proximal tubule. If patients are identified with polycystic kidneys in which cysts are restricted to the cortex, AQP11 would be a good candidate for the responsible gene. Recent identification of the genes responsible for these diseases indicates that all gene products are localized to the cilia of the collecting duct (16). As the proxi-

mal tubule also has cilia, AQP11 may be localized downstream of signaling pathways regulated by cilia.

In summary, we have characterized AQP11 expression in the kidney and found that its disruption produces polycystic kidneys following swelling and vacuolization of the proximal tubule. This is the first report on the role of a member of a new AQP subfamily with unique NPA boxes. Our results suggest that AQP11 will play an important role in vesicular homeostasis. Further analysis of AQP11^{-/-} mice will help determine the specific role of AQP11 and clarify the mechanism for cyst formation in the kidney, which will expand the scope of aquaporins.

ACKNOWLEDGMENTS

This work was supported by Grant-in-Aids for Scientific Research from Ministry of Education, Science, Sports and Culture of Japan (13137209 and 13671124).

REFERENCES

1. Bill, R. M., K. Hedfalk, S. Karlgren, J. G. Mullins, J. Rydstrom, and S. Hohmann. 2001. Analysis of the pore of the unusual major intrinsic protein channel, yeast Fps1p. *J. Biol. Chem.* **276**:36543–36549.
2. Drenth, J. P. H., J. A. Martina, R. van de Kerkhof, J. S. Bonifacio, and J. B. M. J. Jansen. 2005. Polycystic liver disease is a disorder of cotranslational protein processing. *Trends Mol. Med.* **11**:37–42.
3. Elkjaer, M. L., L. N. Nejsum, V. Gresz, T. H. Kwon, U. B. Jensen, J. Frokiaer, and S. Nielsen. 2001. Immunolocalization of aquaporin-8 in rat kidney, gastrointestinal tract, testis, and airways. *Am. J. Physiol. Renal Physiol.* **281**:F1047–F1057.
4. Hara-Chikuma, M., B. Yang, N. D. Sonawane, S. Sasaki, S. Uchida, and A. S. Verkman. 2005. CIC-3 chloride channels facilitate endosomal acidification and chloride accumulation. *J. Biol. Chem.* **280**:1241–1247.
5. Hara-Chikuma, M., Y. Wang, S. E. Guggino, W. B. Guggino, and A. S. Verkman. 2005. Impaired acidification in early endosomes of CIC-5 deficient proximal tubule. *Biochem. Biophys. Res. Commun.* **329**:941–946.
6. Igarashi, P., and S. Somlo. 2002. Genetics and pathogenesis of polycystic kidney disease. *J. Am. Soc. Nephrol.* **13**:2384–2398.
7. Ishibashi, K., S. Sasaki, K. Fushimi, S. Uchida, M. Kuwahara, H. Saito, T. Furukawa, K. Nakajima, Y. Yamaguchi, T. Gojobori, and F. Marumo. 1994. Molecular cloning and expression of a member of the aquaporin family with permeability to glycerol and urea in addition to water expressed at the basolateral membrane of kidney collecting duct cells. *Proc. Natl. Acad. Sci. USA* **91**:6269–6273.
8. Ishibashi, K., M. Kuwahara, and S. Sasaki. 2000. Molecular biology of aquaporins. *Rev. Physiol. Biochem. Pharmacol.* **141**:1–32.
9. Ishibashi, K., M. Kuwahara, Y. Kageyama, S. Sasaki, M. Suzuki, and M. Imai. 2000. Molecular cloning of a new aquaporin superfamily in mammals: AQPX1 and AQPX2, p. 123–126. *In* S. Hohmann and S. Nielsen (ed.), *Molecular biology and physiology of water and solute transport*. Kluwer Academic/Plenum Publishers, New York, N.Y.
10. Ishibashi, K., M. Imai, and S. Sasaki. 2000. Cellular localization of aquaporin 7 in the rat kidney. *Exp. Nephrol.* **8**:252–257.
11. Ishibashi, K., T. Morinaga, M. Kuwahara, S. Sasaki, and M. Imai. 2002. Cloning and identification of a new member of water channel (AQP10) as an aquaglyceroporin. *Biochim. Biophys. Acta* **1576**:335–340.
12. Johanson, U., and K. Gustavsson. 2002. A new subfamily of major intrinsic proteins in plants. *Mol. Biol. Evol.* **19**:456–461.
13. Morinaga, T., M. Nakakoshi, A. Hirao, M. Imai, and K. Ishibashi. 2002. Mouse aquaporin 10 gene (AQP10) is a pseudogene. *Biochem. Biophys. Res. Commun.* **294**:630–634.
14. Murata, K., K. Mitsuoka, T. Hirai, T. Walz, P. Agre, J. B. Heymann, A. Engel, and Y. Fujiyoshi. 2000. Structural determinants of water permeation through aquaporin-1. *Nature* **407**:599–605.
15. Nielsen, S., J. Frokiaer, D. Marples, T. H. Kwon, P. Agre, and M. A. Knepper. 2002. Aquaporins in the kidney: from molecules to medicine. *Physiol. Rev.* **82**:205–244.
16. Pazour, G. J. 2004. Intraflagellar transport and cilia-dependent renal disease: the ciliary hypothesis of polycystic kidney disease. *J. Am. Soc. Nephrol.* **15**:2528–2536.
17. Piwon, N., W. Gunther, M. Schwake, M. R. Bosl, and T. J. Jentsch. 2000. CIC-5 Cl-channel disruption impairs endocytosis in a mouse model for Dent's disease. *Nature* **408**:369–373.
18. Sheridan, A., J. Schwartz, V. Kroshian, A. Tercyak, J. Laraia, S. Masino, and W. Lieberthal. 1993. Renal mouse proximal tubular cells are more susceptible than MDCK cells to chemical anoxia. *Am. J. Physiol.* **265**:F323–F350.
19. Sonawane, N. D., and A. S. Verkman. 2003. Determinants of [Cl⁻] in recycling and late endosomes and Golgi complex measured using fluorescent ligands. *J. Cell Biol.* **160**:1129–1138.
20. Sui, H., B. G. Han, J. K. Lee, P. Walian, and B. K. Jap. 2001. Structural basis of water-specific transport through the AQP1 water channel. *Nature* **414**:872–878.
21. Takata, K., T. Matsuzaki, and Y. Tajika. 2004. Aquaporins: water channel proteins of the cell membrane. *Prog. Histochem. Cytochem.* **39**:1–83.
22. Yamashita, S., and Y. Okada. 2005. Mechanisms of heat-induced antigen retrieval: analyses in vitro employing SDS-PAGE and immunohistochemistry. *J. Histochem. Cytochem.* **53**:13–21.
23. Yang, B., A. Gillespie, E. J. Carlson, C. J. Epstein, and A. S. Verkman. 2001. Neonatal mortality in an aquaporin-2 knock-in mouse model of recessive nephrogenic diabetes insipidus. *J. Biol. Chem.* **276**:2775–2779.
24. Yasui, M., A. Hazama, T. H. Kwon, S. Nielsen, W. B. Guggino, and P. Agre. 1999. Rapid gating and anion permeability of an intracellular aquaporin. *Nature* **402**:184–187.